3D jet simulation using four turbulent model

André Reinaldo Novgorodcev Júnior; Antônio C. P. Brasil Júnior
Universidade de Brasília – Departamento de Engenharia Mecânica – Graduação – Laboratório de Energia e Ambiente – LEA
CEP 70.910-900 – Brasília - DF – Brasil
andrernjr@yahoo.com; brasil@enm.unb.br

Abstract. *The 3D turbulent jet into a cross flow is a classical and complex 3D flow encountered in many industrial applications. In this problem fluid is injected from a round exit with diameter D, velocity I_{vy} in a cross stream with velocity given by U_0. The simulation of the flow is performed at CFX 5.5.1 commercial software, using the finite volume method with a tetrahedrical mesh. Four of the most industrially used turbulent models are adopted in this work and the results are compared with experimental data reported in the literature to determine which model fits better in the study of a 3D turbulent jet. The models adopted are k - ε, k - ω, Reynolds stress, and RNG k - ε turbulence models.*

Keywords*. Numerical simulation, free jet, CFD, turbulence models.*

1. Introduction

The 3D turbulent jet into a cross flow is a classical and complex 3D flow encountered in many industrial applications. In this problem fluid is injected from exit with diameter D, with a velocity V_j in a cross stream with velocity U_0. The study of this flow is related to great number real situations of industrial mixing problems. Mixing devices of chemical industry, flows into combustion chambers of aircraft engines, film cooling of turbine blades and VSTOL flows, are typical examples of this kind of flow.

Many works are reported in the literature concerning the jet in a cross flow. An excellent review is presented by Margason (1993) where the most important works about this problem are analyzed. This review paper evaluates the different features of the 3D flow based in a lot of experimental and numerical results, which have been published during the last 50 year. In the present work experimental results of Crabb et al. (1989) will be used for the comparisons of the results.

The cross-stream jet flow has complex 3D physical characteristics enrolling the relationship between the jet, the free stream and the injection wall. The jet acts as an obstacle to the free stream, producing a recirculation zone in the back region of its body. The wake flow behind the jet in not completely similar to the flow behind obstacles. The recirculation patterns are inhibited by the vertical entrainment provided by the jet flow. The momentum exchange between the jet and the free stream produces a deformation of the jet as a flexible body, aligning it to the stream direction. This deflection, added to the fluid entrainment, induces a secondary flow normal to the trajectory composed by a pair of counterotating vortices. This is a typical pattern of the 3D jet giving a kidney shape to its body. Near to the wall, a horseshoe vortex and a wake vortex street are other important three-dimensional patterns of this flow. The entire set of 3D topological characteristics is very difficult to be simulated by numerical computations. It requires a good discretization of the domain, and realistic turbulent models, mainly to describe the near wall effects.

The topological structures presented in the last paragraph are controlled mainly by inertial and pressure gradients effects, as a consequence of the mean momentum conservation. The hydrodynamic turbulence, in this case, has a secondary hole. Its influence is observed in the near wall region as well as in the wake of the jet. The turbulence influences, weakly, the diffusion of the counterotating vortices and consequently their sizes and their relative positions to the jet trajectory. On the other hand, for the heat transfer the turbulence is very important. Mixing effects in the jet body due to the counteroteting vortices controls the scalar turbulent diffusion.

The main objective of this work is to verify which of the turbulent models used here obtains the better results for the complex 3D patterns of the 3D jet flow.

2. Governing Equations

For incompressible turbulent flow, the conservation of mass, momentum and energy can be expressed by the classical Reynolds Averaged Navier Stokes (RANS) Equations, given by:

$$\nabla U = 0 \tag{1}$$

$$\frac{\partial U}{\partial t} + \nabla(U)U = -\frac{1}{\rho}\nabla P + \nabla \bullet \left(\nu \nabla U - \overline{u \otimes u}\right) \tag{2}$$

$$\frac{\partial \theta}{\partial t} + U\nabla\theta = \alpha\nabla^2\theta - \nabla\left(\overline{u\theta'}\right) \tag{3}$$

In those equations U, P and θ are the mean velocity, pressure and temperature fields; ρ, υ and α are the density, kinematics viscosity and thermal diffusivity of the fluid; and $\overline{u \otimes u}$ is the Reynolds stress tensor modeled by the Boussinesq eddy viscosity assumption, Eq. (4):

$$\overline{u \otimes u} = \frac{2}{3} kI - 2\upsilon_T D(U) \tag{4}$$

where υ_T is the turbulent eddy viscosity, **D**(**U**) is the mean rate-of-strain tensor, **I** is the identity tensor and k is the Kinetic energy of turbulence.

3. Turbulence Models

3.1. k - ε Model

The k-ε (k-epsilon) model, proposed by Jones & Lauder (1972), is the industry standard two-equation turbulence model. k is the turbulence kinetic energy and is defined as the variance of the fluctuations in velocity. It has dimensions of (L^2 T^{-2}), e.g. m^2/s^2. ε is the turbulence eddy dissipation (the rate at which the velocity fluctuations dissipate) and has dimensions of k per unit time (L^2 T^{-3}), e.g. m^2/s^3.

This model is based on the eddy viscosity concept. The turbulent eddy viscosity is modeled by the Prandtl-Kolmogorov relation, Eq. (5):

$$\nu_T = C_\mu \frac{k^2}{\varepsilon} \tag{5}$$

where ε is the dissipation rate of kinetic energy. This model requires the use of two additional transport equations for k and ε given by:

$$\frac{\partial k}{\partial t} + U\nabla k = \nabla.\left[\left(\nu + \frac{\nu_T}{\sigma_k}\right)\nabla k\right] + P_k - \varepsilon \tag{6}$$

$$\frac{\partial \varepsilon}{\partial t} + U\nabla \varepsilon = \nabla.\left[\left(\nu + \frac{\nu_T}{\sigma_\varepsilon}\right)\nabla \varepsilon\right] + C_{\varepsilon 1} P_k \frac{\varepsilon}{k} - C_{\varepsilon 2} \frac{\varepsilon^2}{k} \tag{7}$$

In those equations P_k is the production of k which is written in Eq. (8):

$$P_k = 2\nu_T \left[D(U) : D(U)\right] \tag{8}$$

The standard values of the constants are:

$$C_\mu = 0.09; C_{\varepsilon 1} = 1.44; C_{\varepsilon 2} = 1.92;$$
$$\sigma_k = 1.0; \sigma_\varepsilon = 1.3$$

3.1. RNG k - ε Model

The RNG k-ε model is an alternative to the standard k-ε model. It is based on renormalization group analysis of the Navier-Stokes equations. The transport equations for turbulence generation and dissipation are the same as those for the standard k-ε model, but the model constants differ, and the constant $C_{\varepsilon 1}$ is replaced by the function $C_{\varepsilon 1RNG}$. The transport equation for turbulence dissipation becomes, Eq. (9).

$$\frac{\partial \varepsilon}{\partial t} + U\nabla \varepsilon = \nabla.\left[\left(\nu + \frac{\nu_T}{\sigma_{\varepsilon RNG}}\right)\nabla \varepsilon\right] + C_{\varepsilon 1RNG} P_k \frac{\varepsilon}{k} - C_{\varepsilon 2RNG} \frac{\varepsilon^2}{k}$$

where,

$$C_{\varepsilon 1RNG} = 1.42 - f_\eta \tag{10}$$

and,

$$f_\eta = \frac{\eta\left(1-\frac{\eta}{4.38}\right)}{\left(1+\beta_{RNG}\eta^3\right)} \tag{11}$$

$$\eta = \sqrt{\frac{P_k}{\rho C_{\mu RNG}{}^{\varepsilon}}} \tag{12}$$

The standard values of the constants are:

$$C_{\mu RNG} = 0.085; C_{\varepsilon 2RNG} = 1.68;$$
$$\sigma_{kRNG} = 0.7179; \sigma_{\varepsilon RNG} = 0.7179; \beta_{\mathrm{RNG}} = 0.012$$

3.1. k-ω Model

One of the main problems in turbulence modeling is the accurate prediction of flow separation from a smooth surface. The new models developed to solve this problem have shown a significantly more accurate prediction of separation in a number of test cases and in industrial applications. Currently, the most prominent two-equation models in this area are the *k*-w based models of Menter.

CFX uses the k-ε model developed by Wilcox. The starting point of the present formulation is the *k*-w model developed by Wilcox. It solves two transport equations, one for the turbulent kinetic energy, *k*, Eq. (13) and one for the turbulent frequency, w, Eq. (14). The stress tensor is computed from the eddy-viscosity concept.

$$\frac{\partial(\rho k)}{\partial t} + \nabla \bullet (\rho U k) = P_k - \beta' \nabla \rho k\omega + \nabla \bullet \left[\left(\mu + \frac{\mu_T}{\sigma_k}\right)\nabla k\right] \tag{13}$$

$$\frac{\partial(\rho\omega)}{\partial t} + \nabla \bullet (\rho U \omega) = \alpha \frac{\omega}{k} P_k - \beta \nabla \rho \omega^2 + \nabla \bullet \left[\left(\mu + \frac{\mu_T}{\sigma_\omega}\right)\nabla \omega\right] \tag{14}$$

In addition to the independent variables, the density, r, and the velocity vector, $\boldsymbol{U}$, are treated as known quantities from the Navier-Stokes method. P_k is the production rate of turbulence and is similar to P_k used in the k-ε model. The model constants are given by:

$$\beta' = 0.09; \alpha = 5/9; \beta = 3/40;$$
$$\sigma_k = 2; \sigma_\varepsilon = 2$$

3.1. Reynold Stress Models (RSM)

These models are based on transport equations for all components of the Reynolds stress tensor and the dissipation rate. They are suitable for strongly anisotropic flows. These models do not use the eddy viscosity hypothesis, but solve an equation for the transport of Reynolds stresses in the fluid. The Reynolds stress model transport equations are solved for the individual stress components. Algebraic Reynolds stress models solve algebraic equations for the Reynolds stresses, whereas differential Reynolds stress models solve differential transport equations individually for each Reynolds stress component. In CFX-5 the latter of these is implemented.

The CFX-5 Solver solves the following equations, Eq. (15), for the transport of the Reynolds stresses:

$$\frac{\partial \rho \overline{u \otimes u}}{\partial t} + \nabla \bullet \left(\rho U \otimes \overline{u \otimes u}\right) = P + \underline{\underline{\phi}} + \nabla \bullet \left(\left(\mu + \frac{2}{3} c_S \rho \frac{k^2}{\varepsilon}\right)\nabla \overline{u \otimes u}\right) - \frac{2}{3}\rho\varepsilon\delta \tag{15}$$

where $\underline{\underline{\phi}}$ the pressure-strain correlation, cS is is 0.22 and P, the exact production term, is given by, Eg.(16):

$$P = -\rho\left(\overline{u \otimes u}(\nabla U)^T + (\nabla U)\overline{u \otimes u}\right) \tag{16}$$

4. Boundary conditions

The jet-to-cross-flow ratio was selected to be 2.3 and the jet Reynolds number was 52000. For inflow surfaces the value of velocity, kinetic energy and dissipation fields are predicted. For outlet the relative static pressure over the outlet boundary is specified. In the top wall the value of velocity, kinetic energy and dissipation fields are predicted. In the sidewalls a free slip condition are imposed. In the bottom walls no slip condition are imposed.

Close to the solid boundaries the turbulence model does not hold. The computational domain have to be dislocated at a distance δ from the solid walls and equilibrium laws for mean velocity are imposed for parallel surface. The wall-function approach used is an extension of the method of Launder and Spalding. In the log-law region, the near wall tangential velocity is related to the wall-shear-stress, t_w, by means of a logarithmic relation. The computational domain extends for 6 diameters (6D) from the symmetry axis to a free boundary, in the lateral direction, 6D from the wall to a free boundary, in the vertical direction, 2.5D from de nom-perturbed inlet to the cross flow inlet and 11.5D from the cross flow inlet to exit planes, in the streamwise direction. It is represented in figure (1).

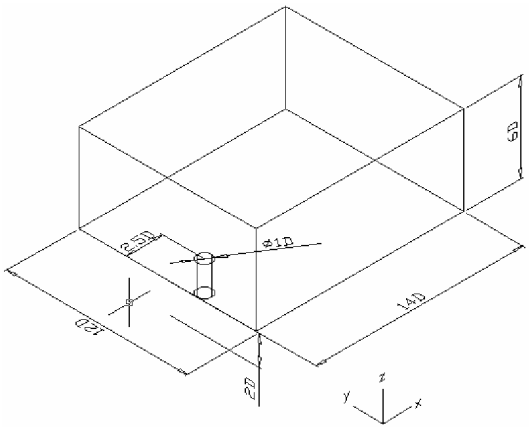

Figure1. Computational domain.

In the computations a non-uniform grid with 607308 nodes is utilized, with most points concentrated in the regions near the jet discharge, in the jet downstream trajectory, and in the symmetry-plane. The grid in the symmetry-plane is represented in fig (2) and in a xy plane passing by the center of the jet (3).

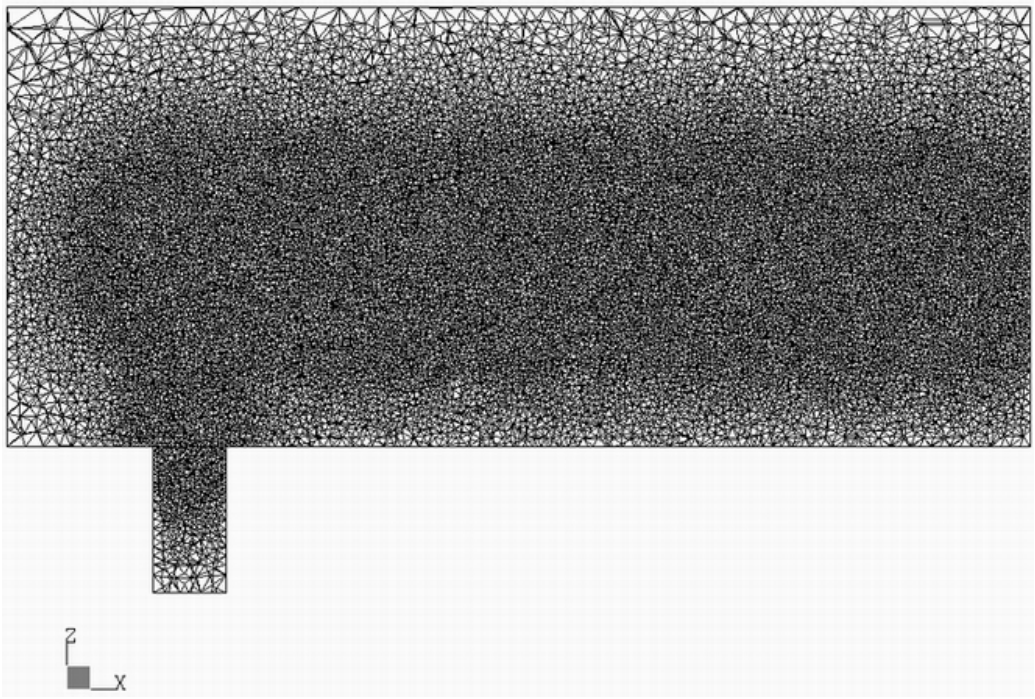

Figure 2. Computational grid in the symmetry-plane.

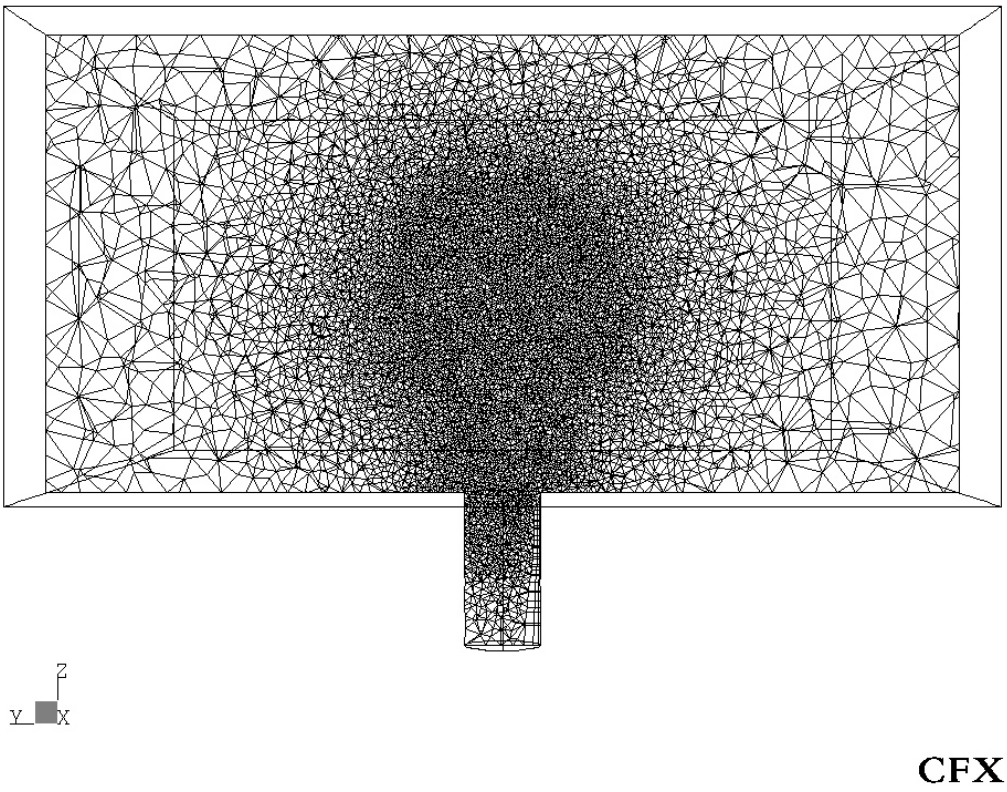

Figure 3. Computational grid in a xy plane passing by the center of the jet.

5. Results

For the classical problem of a 3D round jet injected in a cross flow a great number of experimental data is available. The numerical simulation performed here corresponds to the CRABB´s experiment (jet-to-cross-flow ratio equal to 2.3), where a couplet set of results for mean and turbulent fields are given

The fig. (4) shows the development of the jet in the streamwise direction. The fig. (5) represents a general visualization of the mean velocity vectors in the symmetry and near the wall planes. Qualitatively, the computations can describe all of the most important mean flow structures reported in the previous works, like the formation of Prandtl secondary vortex due to the interaction between the jet and shear, and the recirculation zone behind the jet exit, similar to the near wake of circular obstacle in crossflow.

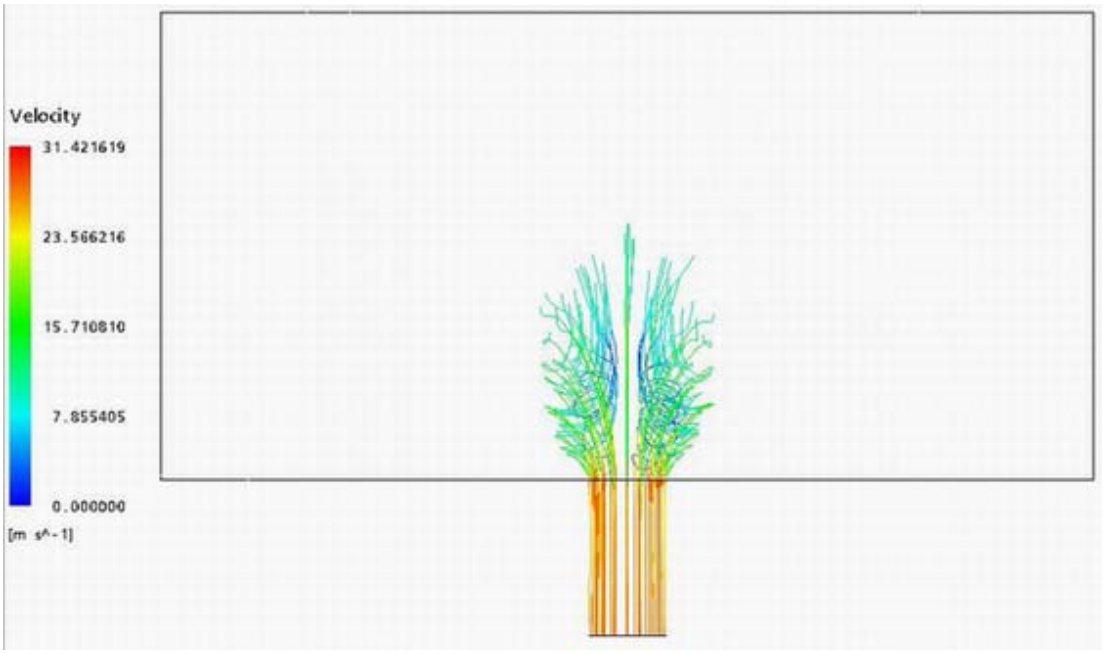

Figure 4. Development of the jet in the streamwise direction.

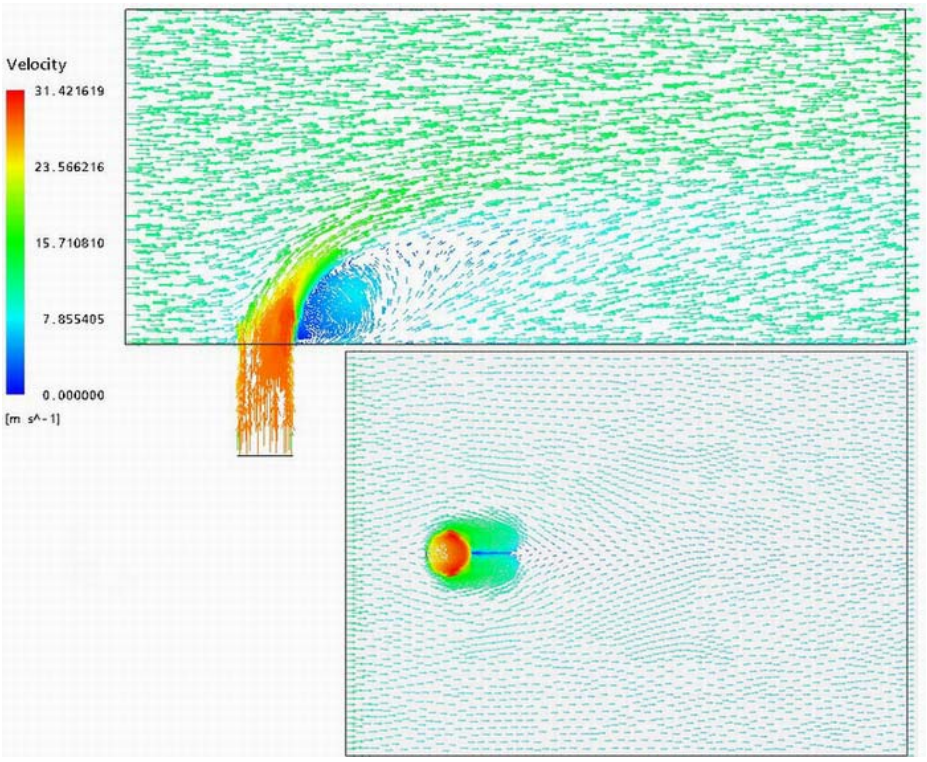

Figure 5. Velocity vectors in the symmetry and near the wall planes.

The computational Jet trajectory agree well with the experimental results and with other numerical works.

The three-dimensional nature of the flowfield is illustrated by the vector fields of Fig. (6), whish shows the secondary velocity fields at different spanwise planes (x/D =1 and 2).It is observed that a counterrotating vortex pair starts to appear at x/D =1 and its straight decreases downstream. Also, the pressure drop in the wake region induces an inward motion, transporting the fluid from the crossflow toward the jet center plane. Thus, at x/D = 1, the somewhat irregular movement near the wall is due to the inward motion, whish is balanced by the outward flow generated by the jet on either sides of the jet exit.

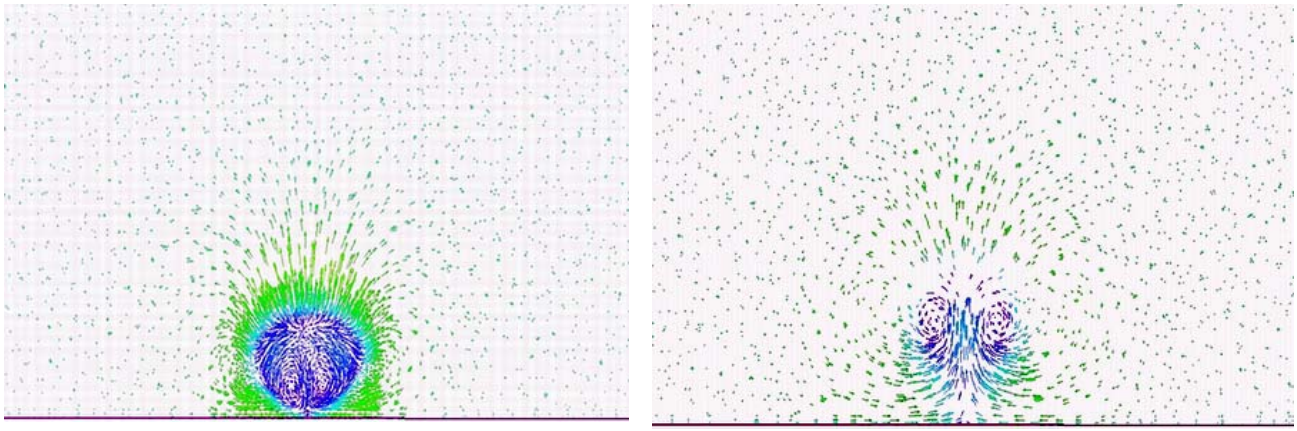

X/D = 1 X/D = 2

Figure 6. Velocity vectors at different spanwise planes.

The streamwise velocity (U) profiles at jet center plane obtained using the different turbulent models are compared in fig. (7) with each other and with the experimental results. At x/D = 1 the results of RNG k-ε and RSM turbulence models are very close and show good agreement with experimental data. At x/D = 2 and x/D = 4 results of k-ε and k-ω become closer to the experimental data. At x/D = 6, where the counterrotating vortex become weaker and the jet is more similar to the non disturbed profile, the results of RNG k-ε and RSM shows better agreement with experimental results.

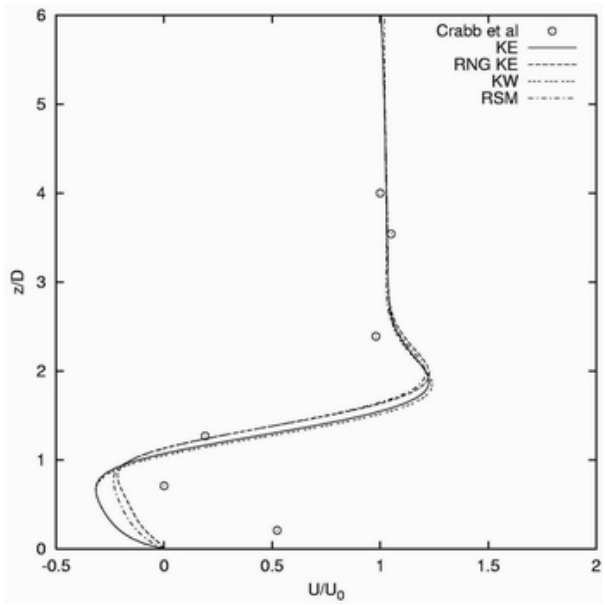

x/D = 1

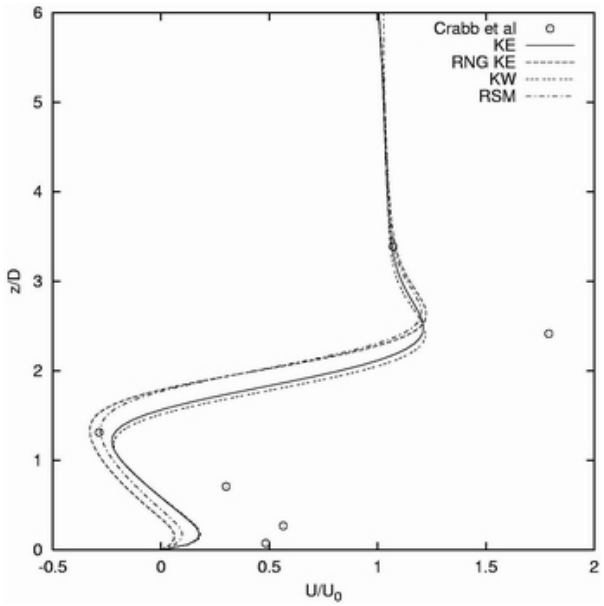

x/D = 2

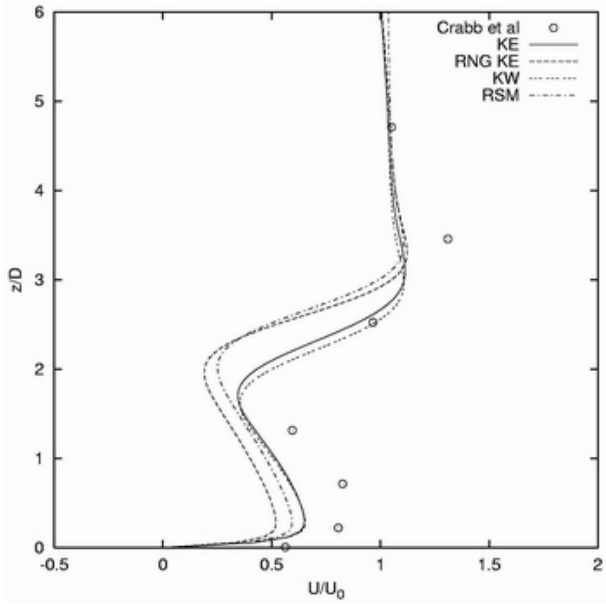

x/D = 4

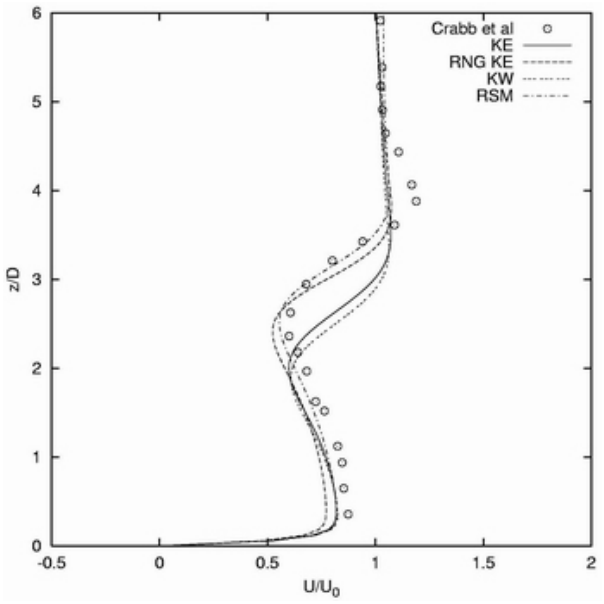

x/D = 6

Figure 7. Streamwise velocity profiles at the jet center plane (y/D = 0)

The streamwise velocity (U) and the crossflow velocity (W) in the symmetry plane obtained using the different turbulent models, for different distances from the floor, z/D = 0.75 (fig. (8)) and z/D = 1.35(fig. (9)), are compared with each other and with the experimental results. At this profiles the k-ε turbulent model show better results, getting closer to the peaks of velocities.

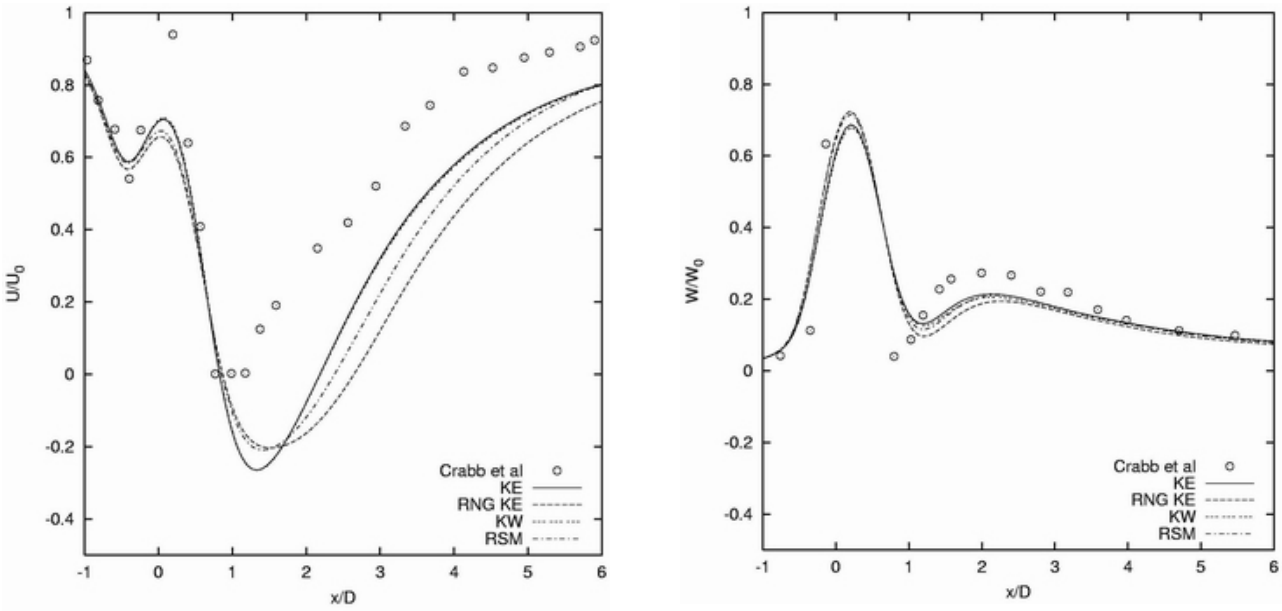

Figure 8. Streamwise velocity and the crossflow velocity in the symmetry plane, z/D = 0.75

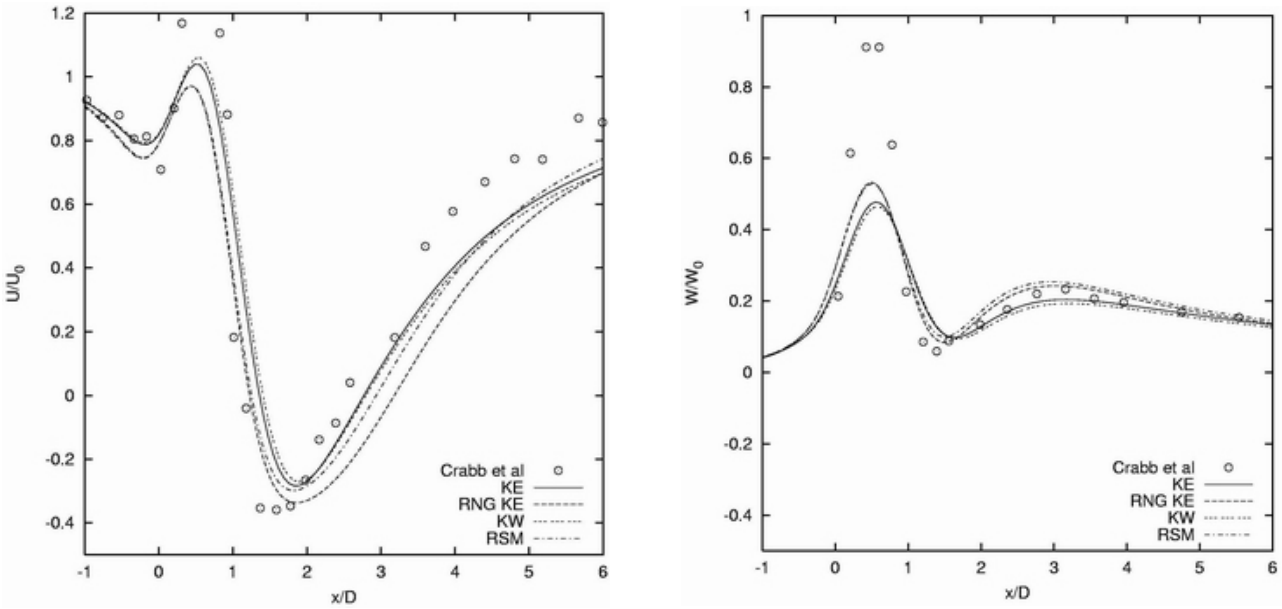

Figure 9. Streamwise velocity and the crossflow velocity in the symmetry plane, z/D = 1.35

In fig. (10) the same results of fig. (8) and (9) are repeated for a plane with a 0.5 D of displacement in relation of the symmetry plane (y/D = 0.5) and in a distance of 0.75D from the floor (z/D=0.75). The numerical results are less accurate them the results obtained in the symmetry plane, but the k-ε turbulent model show the better results again.

An important aspect in numerical simulation is the computational time. In this aspect the k-ε turbulent model was the faster, while the Reynolds Stress Model demanded more computational time, using the same computer.

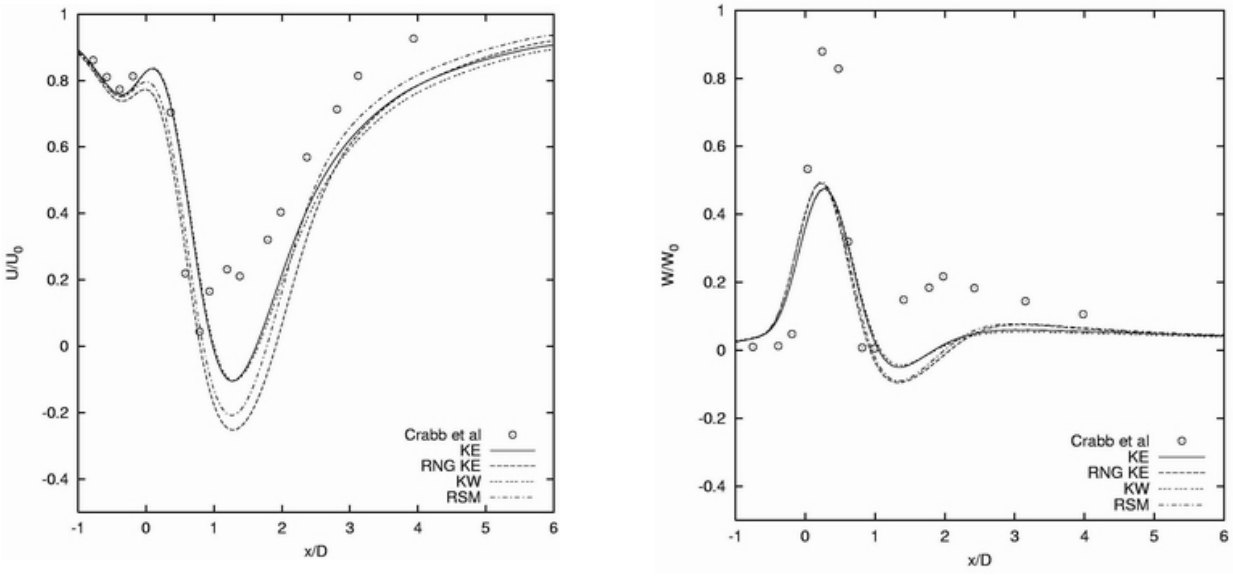

Figure 9. Streamwise velocity and the crossflow velocity in the plane y/D = 0.5, z/D = 0.75

8. Conclusions

In this study, a three-dimensional flowfield of normal jets in a crossflow was computationally simulated. For the turbulence modeling, the k-ε, RNG k-ε, k-ω and Reynolds Stress Model were used. The results of numerical simulation were compared with previous experimental results for the velocity ratio of 2.3

The computational results for the main velocity profiles agreed well with experimental data, whereas there are some differences in the turbulence kinetic energy. The k-ε turbulent model shows the best results for the velocity development profiles and good results in the streamwise velocity profiles. Moreover the k-ε model demands less computational time, saving precious CPU time. This unexpected supremacy of the k-ε model can be credited to the mash and the boundary conditions used. None of the model was able to catch the peaks of velocities and the correct velocity profiles near the floor.

The problem near the floor may be solved refining the mash near the floor, but this solution will demand a more powerful computer.

7. References

Catalano, G.D.; Chang, K.S. and Mathis J.A, 1989, "Investigate of turbulent impingement in a confined crossflow", AIAA journal, 27, 11, pp. 1530-1535.

Patankar, S.V.; Basu, D.K. and Alpay, S.A., 1977, "Prediction of the three-dimensional velocity field of deflected turbulent jet", ASME J. of Fluid Eng., pp. 758-762.

Keimasi, M.R.; Taeibi-Rahni, M., 2001, "Numerical Simulation of Jets in a Crossflow Using Different Turbulence Models", AIAA journal, 39, 12, pp. 2268-2277.

Demuren, O.A., 1993, "Characteristics Of Three-Dimensional turbulent Jets In Crossflow", Int. J. Eqng Sci, 31, 6, pp. 899-913,

Crabb, D.; Durão, D.F.G. and Whiterlaw, J.H., 1981, "A round jet normal to a cross flow", ASME J. of Fluid Eng., pp. 142-153.